Efficient Electromagnetic Scattering Analysis of Open-ended Circular Cavities with Modal MoM Method

A. Aghabarati, P. Dehkhoda, and A. Tavakoli

Department of Electrical Engineering
Amirkabir University of Technology, Tehran, Iran
aghabarati@gmail.com, pdehkhoda@aut.ac.ir, tavakoli@aut.ac.ir

Abstract ─ An efficient and accurate technique is introduced to calculate the scattered electromagnetic (EM) fields from an open-ended circular cavity (OECC). In this paper, it is assumed that the OECC is perforated in an infinite perfect electric conductor (IPEC). Then, the scattered fields are calculated using modal Method of Moments. The complexity and computational cost of the encountered quadruple integrals are addressed in detail. Here, the singularities are extracted and resolved. Next, the scattered far field of a circular PEC plate of the same size is calculated by physical optics approximation. The final OECC scattered field is the sum of these two solutions. A very good agreement is observed between the results of this method and full wave numerical simulations and measurements. The proposed approach is highly efficient and accurate over a wide range of frequencies and incidence angles, making it appealing for analysis of large frequency dispersive structures.

Index Terms ─ Electromagnetic scattering, modal moment method, open-ended circular cavity.

I. INTRODUCTION

Electromagnetic (EM) scattering from open-ended waveguides is an important and challenging problem in applied electromagnetics. Ducts and jet engine inlets that significantly contribute to the total Radar Cross Section (RCS) can be modeled by waveguide structures. The subject is also important in target recognition, object classification, and remote sensing applications.

An informative review of the existing methods for scattering analysis of open-ended cavity structures is presented by Anastassiue [1]. In this review, the methods are classified into two major categories for arbitrary shapes and canonical waveguides. For arbitrary structures, numerical techniques are reported [2-4]. In spite of their generality for handling complex geometries, these methods are computationally limited to small scatterers, particularly in wideband analysis. Various hybrid methods are developed to reduce the computational burden [5-6]. At high frequencies, where the cavity dimensions are large compared to the wavelength, asymptotic methods such as Physical Optics (PO), Soothing and Bouncing Rays (SBR) or the method of Generalized Ray Expansion (GRE) are reported [7-9].

Recently, a full wave approach by using finite-element sub-domain based scattering matrix methodology is proposed for open-ended cavities which aim to solve electrically large problem efficiently by using a reduced-order modeling technique. The efficiency in this model reduction is achieved by changing from finite element degrees of freedom to guided wave participation factors [10, 11].

For open-ended rectangular or circular waveguides, modal methods are utilized to model the wave propagation through the duct [12-14]. Modal analysis is also used to model multi-section inlets or complex terminated geometries containing hubs or straight blades [15, 16]. This efficient method is extensively used with a satisfactory level of accuracy for various cavity problems.

Here, a full wave modal moment technique (modal MoM) is offered to evaluate the scattered fields from an open-ended circular cavity (OECC). First, the modal MoM is employed to calculate the scattered field from an OECC perforated in an infinite perfect electric conductor (IPEC). In this phase, all the mutual couplings between the propagating and evanescent modes excited at the aperture are considered efficiently in the moment admittance matrix. Second, the scattered field from a PEC plate of the same shape and size of the waveguide aperture is calculated by PO method. The two solutions of the scattered fields are added to obtain the scattered field of an OECC.

The total unknown magnetic current on the aperture is represented by an entire domain vector wave function in cylindrical coordinates. The continuity of the magnetic field on the aperture is enforced and the resulted integral equation is solved by Galerkin method.

Here, the computational complexity is carefully addressed by resolving singularities and decreasing the order of integrations.

Monostatic Radar Cross Section (RSC) of various OECCs are calculated and compared with full wave numerical methods and measurements. An excellent

Submitted On: May 25, 2014
Accepted On:July 4, 2016

agreement is observed between the results for both vertical and horizontal polarizations. It is shown that adding the scattered field of the PEC to the results of the waveguide terminated by an IPEC removes the effect of IPEC presence, especially at low grazing angles. This cost effective approach could be used for wideband time-frequency dispersion analysis of open-ended circular cavities.

In Section 2, the mathematical formulation of scattering form an OECC at different polarizations is presented. Section 3 contains the comparison between the results of this approach and Finite Element-Infinite Element (FE-IE) approach [4], the Multi-Level Fast Multipole Method (MLFMM) by the commercial software FEKO and measurements. The concluding remarks are given in Section 4.

II. MATHEMATICAL FORMULATION

In this section, the scattered far field for a real OECC is formulated for an arbitrarily polarized incident plane wave based on modal Method of Moments (modal MoM).

A. Problem description and solution steps

Figure 1 shows a perfect electric conductor OECC. The waveguide is open ended at one side and shorted at the other. L is the length of the cavity and D is its diameter. The goal is the evaluation of the scattered far fields in the $z > 0$ half space, when the cylinder is obliquely illuminated by a plane wave incident at (θ_i, ϕ_i):

$$\vec{\boldsymbol{E}}_{inc} = e^{-j\vec{k}_i\cdot\vec{r}_i}\left(E^{\theta}_{inc}\hat{u}_{\theta} + E^{\phi}_{inc}\hat{u}_{\phi}\right), \quad (1)$$

where,

$$\vec{k}_i = k_0\hat{u}_i = k_0[\cos(\theta_i)\cos(\phi_i)\,\hat{u}_x + \cos(\theta_i)\sin(\phi_i)\,\hat{u}_y + \sin(\theta_i)\,\hat{u}_z], \quad (2)$$

is the wave vector and $k_0 = 2\pi/\lambda_0$ is the free space wave number. We note that the unit for all the angles in the text is radian.

Here, let $a = D/\lambda_0$ be the normalized aperture diameter, $l = L/\lambda_0$ be the normalized cavity length and also $\bar{k} = k_0/\lambda_0$ be the normalized value of wave number with respect to the wavelength.

Due to axial symmetry, one can arbitrarily set $\phi_i = 0$ and then analyze the problem for the perpendicular polarization (TM) and the parallel polarization (TE). In the following derivations, $\parallel$ and $\perp$ represent TE and TM polarizations, respectively as shown in Fig. 2. Dividing the incident wave into two polarizations leads to $E^{\theta}_{inc} = E^{\parallel}_0$ and $E^{\phi}_{inc} = E^{\perp}_0$, as well as explicit expressions for the interior EM fields in terms of modal expansions. Similarly, back scattered field can be represented by a diagonal normalized scattering matrix as in [13]. The backscattered field for the observation point $\vec{r}_s$ is:

$$\vec{\boldsymbol{E}}^{s}(\vec{r}_s) = \boldsymbol{E}^{s\parallel}(\vec{r}_s)\hat{u}_{\theta} + \boldsymbol{E}^{s\perp}(\vec{r}_s)\hat{u}_{\phi}. \quad (3)$$

Now, the problem is solved in two steps as follows:

Step 1: It is assumed that the cavity's aperture is perforated in an IPEC and then EM scattered fields are calculated. Here, applying the surface equivalence principle and enforcing the magnetic field boundary condition on the aperture results in an integral equation with unknown magnetic currents in which the dyadic Green's functions of the circular cavity and the upper half-space are utilized. The magnetic currents on the aperture ($\vec{M}_{\Gamma}$) are expanded in cylindrical entire domain basis functions for evaluation. This derivation is based on an infinite ground plane assumption and is not accurate for a real OECC [17]. However, the modification in step 2 corrects the scattered field calculations.

Step 2: Now, the scattered field of step 1 is corrected using the approach of Zdunek and Rachowicz [17]. The correction is done by adding the PO scattered field of a co-located hypothetical PEC lid of the aperture size to the previously calculated one. The simple modification provided by $\vec{\boldsymbol{E}}^{s}_{lid}(\vec{\boldsymbol{J}}_{\Gamma})$ is shown to be corrective, especially for close to normal incidence angles on the aperture.

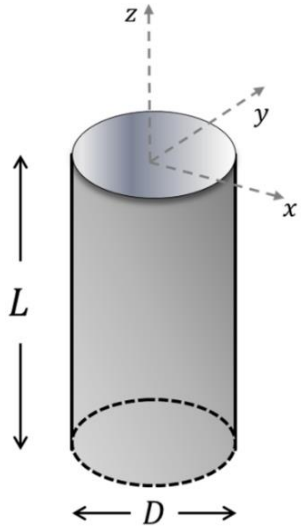

Fig. 1. Geometry of the problem.

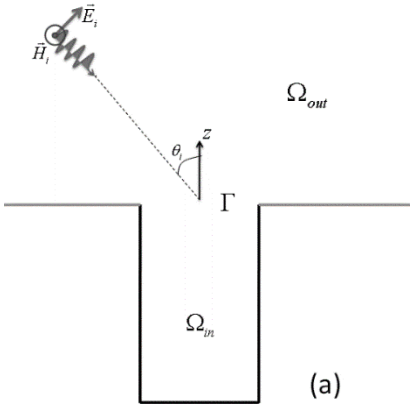

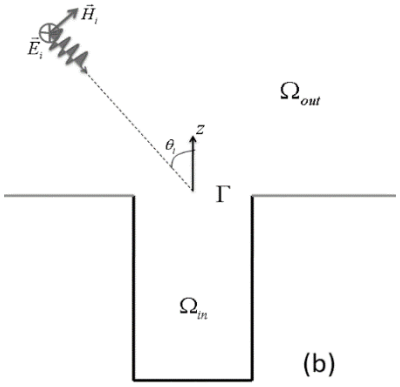

Fig. 2. Perforated OECC in an IPEC, illuminated by: (a) horizontally polarized, and (b) vertical polarized incident wave.

B. Modal MoM solution for an OECC terminated by an IPEC

Here, it is assumed that the aperture of OECC is perforated in an IPEC. This structure is analyzed by modal MoM and is called GP (Ground Plane) model. The unknown electric field on the aperture is expanded by modal functions for the TM and TE polarizations with unknown coefficients as:

$$\vec{\boldsymbol{E}}_{\Gamma}^{\parallel} = \sum_{m=0}^{M}\sum_{n=0}^{N}\left\{C_{nm}^{\mathbf{M^o}}\vec{\mathbf{M}}_{\mu_{nm}}^{\mathbf{o}} + C_{nm}^{\mathbf{N^e}}\vec{\mathbf{N}}_{\lambda_{nm}}^{\mathbf{e}}\right\}, \tag{4}$$

$$\vec{\boldsymbol{E}}_{\Gamma}^{\perp} = \sum_{m=0}^{M}\sum_{n=0}^{N}\left\{C_{nm}^{\mathbf{M^e}}\vec{\mathbf{M}}_{\mu_{nm}}^{\mathbf{e}}\right\}, \tag{5}$$

where $\Gamma = \{\mathrm{r} \in \mathbb{R}^2 : 0 < \rho < \mathrm{D},\ \mathrm{z} = 0\}$ is the domain of the aperture and nm represents the pair of indices for the considered modes [18]. $\vec{\mathbf{M}}_{\mu_{nm}}^{\mathbf{e}}$, $\vec{\mathbf{M}}_{\mu_{nm}}^{\mathbf{o}}$, $\vec{\mathbf{N}}_{\lambda_{nm}}^{\mathbf{e}}$ (and $\vec{\mathbf{N}}_{\lambda_{nm}}^{\mathbf{o}}$) are even and odd modal functions as reported in [18] and shown at the bottom of this page.

In (5), due to the orthogonality between incident wave and $\vec{\mathbf{N}}_{\lambda_{nm}}^{\mathbf{o}}$ on the aperture, all corresponding excitation coefficients are zero. In (6) and (7), $J_n(\cdot)$ and $J_n'(\cdot)$ are the Bessel function of first kind and its derivative with $\mathcal{Z}_{nm}$ and $\mathcal{Z}_{nm}'$ as their zeroes respectively. We define $\lambda_{nm} = 2\mathcal{Z}_{nm}/\mathrm{D}$ and $\mu_{nm} = 2\mathcal{Z}_{nm}'/\mathrm{D}$. In addition, Π_{nm} and Π_{nm}' are normalization factors for transverse components of nmth TE or TM mode respectively;

$$\Pi_{nm} = \left[J_n'(\mathcal{Z}_{nm})\sqrt{0.5\pi\mathcal{Z}_{nm}^2(1+\delta_n)}\right]^{-1}, \tag{8}$$

$$\Pi_{nm}' = \left[J_n(\mathcal{Z}_{nm}')\sqrt{0.5\pi(\mathcal{Z}_{nm}'^2 - n^2)(1+\delta_n)}\right]^{-1}, \tag{9}$$

where δ_n is the Dirac delta function.

The external and internal regions are separated by an equivalent magnetic currents on the aperture using the equivalence principle. The equivalent magnetic currents are:

$$\vec{\boldsymbol{M}}_{\Gamma}^{\parallel} = \hat{z} \times \vec{\boldsymbol{E}}_{\Gamma}^{\parallel} = \sum_{m=0}^{M}\sum_{n=0}^{N}\left\{C_{nm}^{\mathbf{M^o}}\vec{\mathbf{N}}_{\mu_{nm}}^{\mathbf{o}} - C_{nm}^{\mathbf{N^e}}\vec{\mathbf{M}}_{\lambda_{nm}}^{\mathbf{e}}\right\}, \tag{10}$$

$$\vec{\boldsymbol{M}}_{\Gamma}^{\perp} = \hat{z} \times \vec{\boldsymbol{E}}_{\Gamma}^{\perp} = -\sum_{m=0}^{M}\sum_{n=0}^{N}\left\{C_{nm}^{\mathbf{M^e}}\vec{\mathbf{N}}_{\mu_{nm}}^{\mathbf{e}}\right\}. \tag{11}$$

TE and TM Magnetic fields in the internal region ($\Omega_{\mathrm{in}} = \{\mathrm{r} \in \mathbb{R}^3 : 0 < \rho < \mathrm{D}, -\mathrm{L} < \mathrm{z} < 0\}$) are calculated from the sources in (10) and (11) using $\overline{\overline{\mathrm{G}}}_{\mathrm{E}'}$, which is the circular cavity dyadic Green's function of the second kind [18]. The Dyadic Green's function can be used to calculate the magnetic fields due to arbitrary oriented magnetic current source inside the cavity. It is obtained from the solution of vector eigenfunctions in cylindrical coordinate system satisfying the boundary conditions of the cylindrical cavity and provides the basic mathematical tool for numerical study of the cylindrical cavities by MoM. The resultant magnetic fields at $\mathrm{z} = 0$ are:

$$\vec{\boldsymbol{H}}_{\mathrm{in}}^{\parallel}\big|_{z=0} = -\sum_{m=0}^{M}\sum_{n=0}^{N}\left\{\frac{\bar{h}_{nm}^{\mu}\cot(\bar{h}_{nm}^{\mu}l/a)}{\bar{k}^2}C_{nm}^{\mathbf{M^o}}\vec{\mathbf{N}}_{\mu_{nm}}^{\mathbf{e}} - \frac{\cot(\bar{h}_{nm}^{\lambda}l/a)}{\bar{h}_{nm}^{\lambda}}C_{nm}^{\mathbf{N^e}}\vec{\mathbf{M}}_{\lambda_{nm}}^{\mathbf{e}}\right\}, \tag{12}$$

$$\vec{\boldsymbol{H}}_{\mathrm{in}}^{\perp}\big|_{z=0} = -\sum_{m=0}^{M}\sum_{n=0}^{N}\left\{\frac{\bar{h}_{nm}^{\mu}\cot(\bar{h}_{nm}^{\mu}l/a)}{\bar{k}^2}C_{nm}^{\mathbf{M^e}}\vec{\mathbf{N}}_{\mu_{nm}}^{\mathbf{e}}\right\}, \tag{13}$$

where $\bar{h}_{nm}^{\mu} = \sqrt{\bar{\mathrm{k}}^2 - \mathcal{Z}_{nm}'^2}$, $\bar{h}_{nm}^{\lambda} = \sqrt{\bar{\mathrm{k}}^2 - \mathcal{Z}_{nm}^2}$ and $\vec{\mathbf{N}}_{\mu_{nm}}^{\mathbf{e}} = \begin{Bmatrix}\vec{\mathbf{N}}_{\mu_{nm}}^{\mathbf{e}} \\ \vec{\mathbf{N}}_{\mu_{nm}}^{\mathbf{o}}\end{Bmatrix}$ stands for simultaneous inclusion of both even and odd functions.

The magnetic current for the external region ($\Omega_{\mathrm{in}} = \{\mathrm{r} \in \mathbb{R}^3 : \mathrm{z} > 0\}$) is the negative of (10) and (11) due to the continuity of the tangential electric field. Addition of IPEC to the problem allows the application of the half-space Green's function. Magnetic fields at $\mathrm{z} = 0$ become:

$$\vec{\boldsymbol{H}}_{\mathrm{out}}^{\parallel}\big|_{z=0} = \frac{-2}{a}\iint_{\Gamma}\left(1 + \frac{1}{k_0^2}\nabla\nabla\cdot\right)\vec{\boldsymbol{M}}_{\Gamma}^{\parallel}\,\mathbf{G}_0(\vec{\boldsymbol{r}},\vec{\boldsymbol{r}}')\mathrm{d}s', \tag{14}$$

$$\vec{\boldsymbol{H}}_{\mathrm{out}}^{\perp}\big|_{z=0} = \frac{2}{a}\iint_{\Gamma}\left(1 + \frac{1}{k_0^2}\nabla\nabla\cdot\right)\vec{\boldsymbol{M}}_{\Gamma}^{\perp}\,\mathbf{G}_0(\vec{\boldsymbol{r}},\vec{\boldsymbol{r}}')\mathrm{d}s', \tag{15}$$

where $\mathrm{G}_0(\vec{\mathrm{r}},\vec{\mathrm{r}}') = \frac{\mathrm{e}^{\mathrm{j}\mathrm{k}|\vec{\mathrm{r}}-\vec{\mathrm{r}}'|}}{4\pi|\vec{\mathrm{r}}-\vec{\mathrm{r}}'|}$, and the surface integral is

$$\begin{Bmatrix}\vec{\mathbf{M}}_{\mu_{nm}}^{\mathbf{e}} \\ \vec{\mathbf{M}}_{\mu_{nm}}^{\mathbf{o}}\end{Bmatrix} = \Pi_{nm}'\left[\frac{n}{\rho}J_n(\mu_{nm}\rho)\begin{Bmatrix}-\sin(n\phi) \\ \cos(n\phi)\end{Bmatrix}\hat{u}_{\rho} - \mu_{nm}J_n'(\mu_{nm}\rho)\begin{Bmatrix}\cos(n\phi) \\ \sin(n\phi)\end{Bmatrix}\hat{u}_{\phi}\right], \tag{6}$$

$$\begin{Bmatrix}\vec{\mathbf{N}}_{\lambda_{nm}}^{\mathbf{e}} \\ \vec{\mathbf{N}}_{\lambda_{nm}}^{\mathbf{o}}\end{Bmatrix} = \Pi_{nm}\left[\lambda_{nm}J_n'(\lambda_{nm}\rho)\begin{Bmatrix}\cos(n\phi) \\ \sin(n\phi)\end{Bmatrix}\hat{u}_{\rho} - \frac{n}{\rho}J_n(\lambda_{nm}\rho)\begin{Bmatrix}\sin(n\phi) \\ -\cos(n\phi)\end{Bmatrix}\hat{u}_{\phi}\right]. \tag{7}$$

taken over the aperture.

The continuity of the tangential magnetic field at $z = 0$ leads to:

$$\vec{H}^{\parallel,\perp}_{\text{in}}\big|_{z=0} - \vec{H}^{\parallel,\perp}_{\text{out}}\big|_{z=0} = 2\vec{H}^{\parallel,\perp}_{\text{inc}}\big|_{z=0}. \quad (16)$$

Factor 2 in (16) comes from the summation of the incident and reflected fields in the external region. Equation (16) is a Magnetic Field Integral Equation (MFIE) and can be converted to matrix equations using the Galerkin method. The matrix equations have the form $[K]^{\parallel}[C]^{\parallel} = [B]^{\parallel}$ and $[K]^{\perp}[C]^{\perp} = [B]^{\perp}$, where $[K]^{\parallel}$ and $[K]^{\perp}$ are the moment admittance matrices and $[B]^{\parallel}$ and $[B]^{\perp}$ are the excitation matrices. Also, $[C]^{\parallel}$ and $[C]^{\perp}$ consist of the unknown modal amplitudes for the two polarizations that depend on the incident wave angle.

C. Mathematical consideration in admittance and excitation matrices

The above matrices have the following general forms for the two polarizations:

$$\begin{bmatrix} K^{\langle \mathbf{M^e},\mathbf{M^e}\rangle} & K^{\langle \mathbf{M^e},\mathbf{N^o}\rangle} \\ K^{\langle \mathbf{N^o},\mathbf{M^e}\rangle} & K^{\langle \mathbf{N^o},\mathbf{N^o}\rangle} \end{bmatrix} \begin{bmatrix} C^{\mathbf{N^e}} \\ C^{\mathbf{M^o}} \end{bmatrix} = \begin{bmatrix} B^{\langle \mathbf{N^e},\vec{H}^{\parallel}_{\text{inc}}\rangle} \\ B^{\langle \mathbf{N^o},\vec{H}^{\parallel}_{\text{inc}}\rangle} \end{bmatrix}, \quad (17)$$

$$\left[K^{\langle \mathbf{N^o},\mathbf{N^o}\rangle}\right]\left[C^{\mathbf{M^e}}\right] = \left[B^{\langle \mathbf{N^e},\vec{H}^{\perp}_{\text{inc}}\rangle}\right]. \quad (18)$$

Since computing admittance and excitation matrix for the entire domain moment method can impose large computational burden, it is necessary to evaluate them efficiently. The admittance matrices in TE polarization is a block structured matrix. The elements in $[K]^{\parallel}$ and $[K]^{\perp}$ correspond to different interactions between expansion and weighting functions in Galerkin method. Hence, if $W_{pq}(\rho,\phi)$ and $E_{nm}(\rho',\phi')$ are the pqth weighting coefficient and nmth expansion functions, each element of admittance matrices in $[K]^{\parallel}$ or $[K]^{\perp}$ will have the following form:

$$K^{\langle \mathbf{W}_{pq},\mathbf{E}_{nm}\rangle} = V^{\langle \mathbf{W}_{pq},\mathbf{E}_{nm}\rangle} + Z^{\langle \mathbf{W}_{pq},\mathbf{E}_{nm}\rangle}, \quad (19)$$

where $V^{\langle \mathbf{W}_{pq},\mathbf{E}_{nm}\rangle}$ and $Z^{\langle \mathbf{W}_{pq},\mathbf{E}_{nm}\rangle}$ are related to inside and outside field contributions, respectively. Then,

$$V^{\langle \mathbf{W}_{pq},\mathbf{E}_{nm}\rangle} = \iint_{\Gamma}\iint_{\Gamma'} \mathbf{W}_{pq}\cdot\mathbf{E}_{nm}\,ds'\,ds, \quad (20)$$

$$Z^{\langle \mathbf{W}_{pq},\mathbf{E}_{nm}\rangle} = \frac{2}{a}\iint_{\Gamma}\iint_{\Gamma'}\left\{\mathbf{W}_{pq}\cdot\mathbf{E}_{nm} - \frac{1}{k_0^2}\left[\nabla\cdot\mathbf{W}_{pq}\right]\cdot\left[\nabla'\cdot\mathbf{E}_{nm}\right]\right\}\mathbf{G}_0\,ds'ds, \quad (21)$$

where,

$$\langle \mathbf{W}_{pq},\mathbf{E}_{nm}\rangle \in \left\{\begin{matrix}\langle \vec{\mathbf{M}}^{\mathbf{e}}_{\lambda_{pq}},\vec{\mathbf{M}}^{\mathbf{e}}_{\lambda_{nm}}\rangle, \langle \vec{\mathbf{M}}^{\mathbf{e}}_{\lambda_{pq}},\vec{\mathbf{N}}^{\mathbf{o}}_{\mu_{nm}}\rangle, \langle \vec{\mathbf{N}}^{\mathbf{o}}_{\mu_{pq}},\vec{\mathbf{M}}^{\mathbf{e}}_{\lambda_{nm}}\rangle \\ \langle \vec{\mathbf{N}}^{\mathbf{o}}_{\mu_{pq}},\vec{\mathbf{N}}^{\mathbf{o}}_{\mu_{nm}}\rangle, \langle \vec{\mathbf{N}}^{\mathbf{e}}_{\mu_{pq}},\vec{\mathbf{N}}^{\mathbf{e}}_{\mu_{nm}}\rangle\end{matrix}\right\}. \quad (22)$$

While numerical evaluation of (20) is straight forward, evaluation of (21) is complicated due to a singularity at $\vec{r} = \vec{r}'$ in $G_0(\vec{r},\vec{r}')$. By applying the following modifications, the singularity in (21) is removed and the integrations are computed efficiently.

First, at each integration point (ρ,ϕ) in (21), a change of variables $x' - \rho\cos(\phi) = \rho'\cos(\phi')$ and $y' - \rho\sin(\phi) = \rho'\sin(\phi')$ is done in prime coordinates in order to shift the origin into the point (ρ,ϕ). Even though this makes the prime variable integration dependent on ρ and ϕ, but removes the singularity. Next, the integration on ϕ is simply carried out analytically and hence, the order of integration is decreased by one. In addition, orthogonality of the functions with unequal p and n, which leads to zero entries in most of the elements in $[K]^{\parallel}$ and $[K]^{\perp}$, is employed. For instance, outside field contributions of a single element in $K^{\langle \mathbf{N^o},\mathbf{N^o}\rangle}$ can be reduced to the triple integral as follows:

$$Z^{\langle \vec{\mathbf{N}}^{\mathbf{o}}_{\mu_{pq}},\vec{\mathbf{N}}^{\mathbf{o}}_{\mu_{nm}}\rangle} = \delta(p-n)\Pi'_{pq}\Pi'_{nm}\int_{\rho=0}^{1} d\rho \int_{\phi'=0}^{\pi} d\,\phi' \int_{\rho=0}^{\Upsilon} \{[-Z'_{pq}Z'_{pm}J_{p-1}(Z'_{pq}\rho) + \frac{pZ'_{pm}}{\rho}J_p(Z'_{pq}\rho)]J_{p+1}(Z'_{pm}|X|) + [\frac{pZ'_{pq}}{|X|}J_{p-1}(Z'_{pq}\rho) - \left(\frac{Z'_{pq}Z'_{pm}}{2\pi\rho}\right)^2 J_p(Z'_{pq}\rho)]J_p(Z'_{pm}|X|)\} \cos(px)\, e^{j2\pi a\rho'} d\rho', \quad (23)$$

where, $X = \rho + \rho' e^{j\phi'} = |X|e^{jx}$ and $\Upsilon = -\rho\cos(\phi') + \sqrt{1-\rho^2\sin(\phi')}$ are defined variables that appear in the evaluation of non-zero entries for all blocks of admittance matrices. The adaptive quadrature integration method of [19] is used to compute integrations similar to (23) for $[K]^{\parallel}$ and $[K]^{\perp}$.

Here we note that mentioned modifications to the integrals of form (21) extensively reduce the computational cost in modal MoM solution. In contrast to other numerical methods (e.g., sub-domain MoM), this technique deals with a fairly small, sparse, symmetric and well-conditioned matrices. Furthermore, most of the computational cost in this method is due to the calculation of the wave coupling through the aperture, which is independent of the cavity depth or the incident wave direction. Thus, the method is very efficient even for very long dispersive OECCs.

Finally, elements of the excitation matrices are:

$$B^{\langle \mathbf{W}_{pq},\vec{H}^{\parallel}_{\text{inc}}\rangle} = \iint_{\Gamma} \mathbf{W}_{pq}\cdot\vec{H}^{\parallel}_{\text{inc}}\,ds, \quad (24)$$

$$B^{\langle \mathbf{W}_{pq},\vec{H}^{\perp}_{\text{inc}}\rangle} = \iint_{\Gamma} \mathbf{W}_{pq}\cdot\vec{H}^{\perp}_{\text{inc}}\,ds. \quad (25)$$

Integrals in (24) and (25) are analytically evaluated. In horizontal illumination where,

$$\vec{H}^{\parallel}_{\text{inc}} = \frac{-E_0^{\parallel}}{\eta_0}\left(\sin(\phi)\hat{u}_{\rho} + \cos(\phi)\hat{u}_{\phi}\right). \quad (26)$$

The excitation vector is:

$$B^{\langle \vec{\mathbf{N}}^{\mathbf{o}}_{\mu_{pq}},\vec{H}^{\parallel}_{\text{inc}}\rangle} = -4\pi E_0^{\parallel}\Pi'_{pq}(-j)^{p-1}\frac{pJ_p(Z'_{pq})J_p(2\pi a\sin\theta_i)}{2\pi a\sin\theta_i}. \quad (27)$$

D. Evaluation of the scattered field

By solving the matrix equation of (17) and (18), unknown equivalent magnetic currents are obtained. Using the image theory and the free half space Green's function, the total backscattered fields for both polarizations at distance $\bar{r}_s = r/\lambda_0$ and direction of θ_s are:

$$\vec{E}^{s\parallel}_{cavity}(\vec{M}_\Gamma) = -E_0^{\parallel}\frac{ae^{2\pi\bar{r}_s}}{\bar{r}_s} \tag{28}$$
$$\times \sum_{m=0}^{M}\sum_{n=0}^{N}\left\{\begin{array}{l} C^{\mathbf{M^o}}_{nm}\Pi'_{nm}(-j)^{n-1}\dfrac{nJ_n(\mathcal{Z}'_{nm})J_n(\bar{k}\sin\theta_s)}{\bar{k}\sin\theta_s} \\ +C^{\mathbf{N^e}}_{nm}\Pi_{nm}(-j)^{n-1}\dfrac{I_n(\mathcal{Z}_{nm},\bar{k}\sin\theta_s)}{\bar{k}\sin\theta_s}\end{array}\right\},$$

$$\vec{E}^{s\perp}_{cavity}(\vec{M}_\Gamma) = E_0^{\perp}\frac{ae^{2\pi\bar{r}_s}}{\bar{r}_s} \tag{29}$$
$$\times \sum_{m=0}^{M}\sum_{n=0}^{N}\left\{C^{\mathbf{M^e}}_{nm}\Pi'_{nm}(-j)^{n-1}\cos\theta_s\frac{I_n(\mathcal{Z}'_{nm},\bar{k}\sin\theta_s)}{\bar{k}\sin\theta_s}\right\},$$

where $I_n(\cdot,\cdot)$ is a frequently encountered integral in the equations, defied as:

$$I_n(x,y) = \int_0^1 \left\{(n/\rho)^2 J_n(x\rho)J_n(y\rho) + xyJ'_n(x\rho)J'_n(y\rho)\right\}\rho d\rho. \tag{30}$$

E. Scattered field of a real OECC

The interior scattered fields computed from (28) and (29) are the dominant part of the total scattered signal [9]. Even though assumption of an IPEC simplifies the analysis, but it degrades the results, especially at grazing angles [13]. The results could be corrected by adding the PO solution of the scattered field from a hypothetical PEC plate at the aperture:

$$\vec{E}^{s\parallel,\perp}_{total} = \vec{E}^{s\parallel,\perp}_{cavity}(\vec{M}_\Gamma) + \vec{E}^{s\parallel,\perp}_{lid}(\vec{J}_\Gamma), \tag{31}$$

where

$$\begin{Bmatrix}\vec{E}^{s\parallel}_{lid}(\vec{J}_\Gamma)\\ \vec{E}^{s\perp}_{lid}(\vec{J}_\Gamma)\end{Bmatrix} = \frac{j\bar{k}e^{2\pi\bar{r}_s}J_1[\bar{k}(\sin\theta_i+\sin\theta_s)]}{2\pi\bar{r}_s\bar{k}(\sin\theta_i+\sin\theta_s)}\begin{Bmatrix}E_0^{\parallel}\cos\theta_s\\ E_0^{\perp}\cos\theta_s\end{Bmatrix}. \tag{32}$$

From now, $\vec{E}^{s\parallel,\perp}_{\text{total}}$ is referred to modal MoM3D model in the text.

III. NUMERICAL RESULTS

In this section, the monostatic RCS of various targets are evaluated for horizontal and vertical polarizations. The results are compared with Finite Element Method (FEM) [13], Multi-Level Fast Multipole Method (MLFMM) generated by the commercial software FEKO and measurements [20], [21] as well. Generally, measurements are conducted in the anechoic chamber by placing the OECC as a target in front of the standard gain horn antenna, while absorbing materials are used to diminish scattering from the exterior of the cavity to reduce its contribution in the total scattering.

In large waveguides, shooting and bouncing rays method [13] is used for validation. For large apertures or low grazing angles, the field modes m and n should be large enough to assure convergence.

First, a circular cavity with $D = 2\lambda$, $L = 4\lambda$ and $\lambda = 3$ cm is analyzed. Figure 3 shows the monostatic RCS for horizontal illumination as a function of θ_i for $m = 8$ and $n = 10$. The result of modal MoM without correction (GP model) is also shown in Fig. 3. The correction is effective at all incidence angles. Please note that the presence of IPEC underestimates the RCS. The results of FEM [15], FEKO and measurements [20] show a very good agreement with this efficient method.

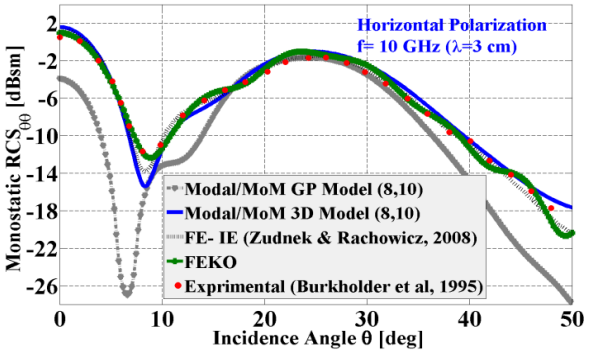

Fig. 3. Horizontal polarization monostatic RCS (dB/m^2) of an OECC with $D = 2\lambda, L = 4\lambda$ versus incidence angle.

Figure 4 depicts the convergence of RCS results for various modes for vertical polarization at 10 GHz as a function of incidence angle. As expected, as incidence angle increases, a larger number of modes are needed for convergence. Considering the hierarchy of the moment matrix, as the number of modes increase, we only need to add the computations of the new modes because previously computed and stored entries are still valid.

Monostatic RCS for the same OECC for vertical polarization is compared to reference methods in Fig. 5. A good agreement between these methods is observed.

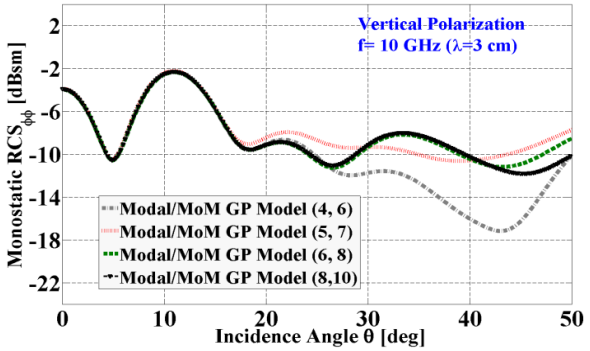

Fig. 4. Convergence of RCS with increasing the number of modes for an OECC with $D = 2\lambda$, $L = 4\lambda$ illuminated by a vertically polarized incident wave.

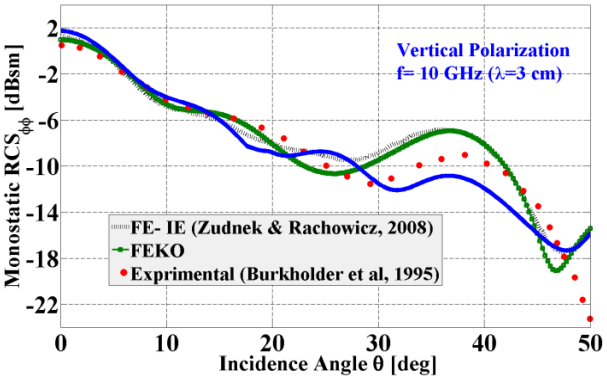

Fig. 5. Vertical polarization monostatic RCS (dB/m^2) of an OECC with $D = 2\lambda$, $L = 4\lambda$ versus incidence angle.

It should be noted that modal MoM is highly accurate and computationally efficient. Due to the similarity of formulations of the two polarizations, entries of matrices could be evaluated at the same time.

For example, $Z^{\langle \vec{N}^e_{\mu pq}, \vec{N}^e_{\mu nm} \rangle}$ and $Z^{\langle \vec{N}^o_{\mu pq}, \vec{N}^o_{\mu nm} \rangle}$ in corresponding blocks of $K^{\langle N^e, N^e \rangle}$ and $K^{\langle N^o, N^o \rangle}$ can be computed simultaneously. This significantly reduces the computational time. CPU time for the RCS calculation of the above OECC for both polarizations is 84.22 sec, while the same simulation with FEKO using MLFMM is about 28 minutes on an Acer Aspire 1.66 GHz laptop with 2GB of RAM.

As a second example, a straight circular cylindrical air-intake channel with $D = 6.274$ cm and $L = 21.59$ cm is analyzed. Convergence is achieved by 54 modes ($m = 4$ and $n = 6$) of horizontal and 56 modes ($m = 6$ and $n = 8$) of vertical polarizations. The same problem is studied in [17] by FE-IE and in [21] with internal irradiation and diffraction model. Measurements are also reported in [17]. Figure 6 shows comparisons of RCS at 15.2 GHz. A very good agreement is observed between these methods at both polarizations.

For the above OECC, the relative amplitude of various modes in horizontal polarization is plotted in Fig. 7.

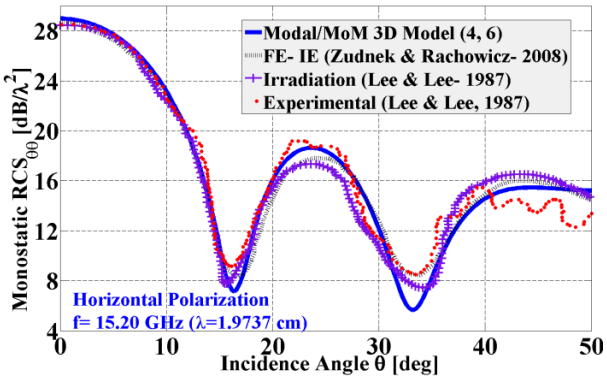

(a)

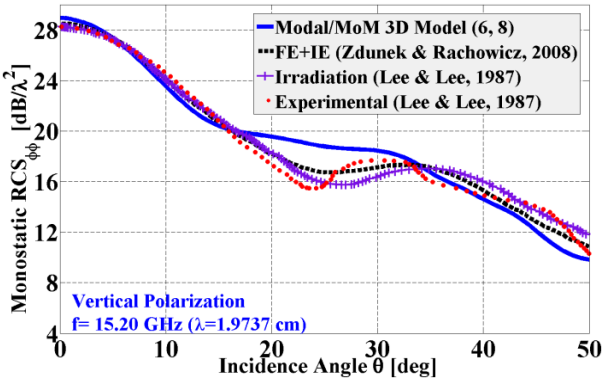

(b)

Fig. 6. Monostatic RCS versus incidence angle for a cylindrical PEC cavity $D = 6.274\ cm$ and $L = 21.59\ cm$: (a) horizontal polarization, and (b) vertical polarization.

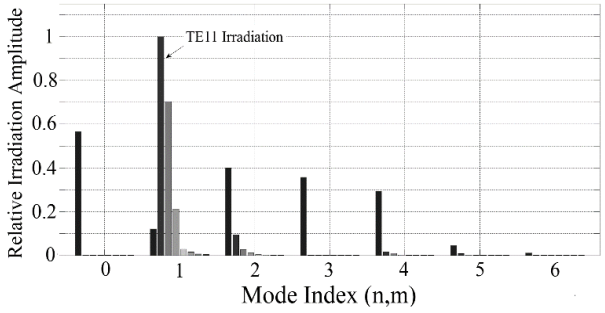

Fig. 7. Comparison of the relative amplitude of irradiating modes in vertical polarization.

Irradiation amplitude of each component is normalized to the dominant propagating mode value, TE_{11}. As observed, higher order vanescent modes might even have some contributions in the total scattered field. Sparsity pattern (non-zero element plot) of moment matrix for vertical polarization is depicted in Fig. 8. For this problem, $[K]^{\|}$ is a 54×54 sparse matrix with 612 non-zeros (%21), while the condition number is 34.9902. As mentioned before, the modal MoM admittance matrix is symmetrical and well-conditioned. Even though the size of $[K]^{\|}$ is favourably small, the above mentioned properties further expedites the numerical solution by using direct or iterative methods.

As another example, a cylindrical large cavity with $D = 10\lambda$ and $D = 30\lambda$ at 10 GHz is considered. This structure is also studied by Ling et al. with SBR method [13]. RCS results are shown in Figs. 9 and 10 at both polarizations. For this large structure, the modes corresponding to $m = 10$ and $n = 14$ yield convergent results. As mentioned before, the computational burden for this long cavity is mainly due to computing the coupling on the aperture and not the cavity length.

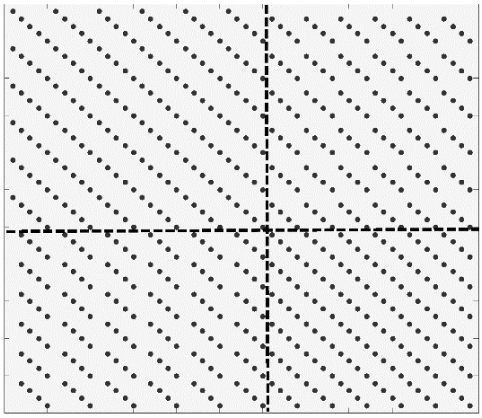

Fig. 8. Sparsity pattern of admittance matrix in modal MoM solution for horizontal polarization.

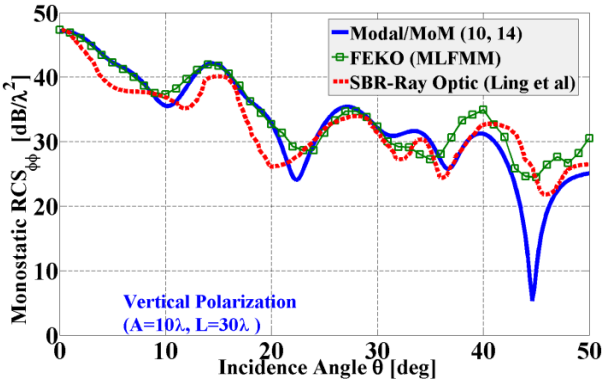

Fig. 9. Monostatic RCS of an OECC with $D = 10\lambda$ and $L = 30\lambda$ versus incidence angle for horizontal polarization.

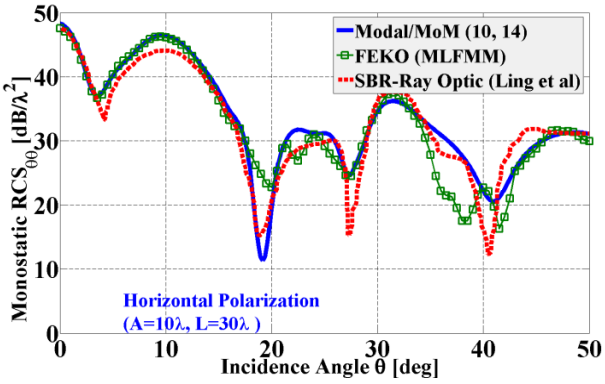

Fig. 10. Monostatic RCS of an OECC with $D = 10\lambda$ and $L = 30\lambda$ versus incidence angle for vertical polarization.

IV. CONCLUSION

Here, an efficient technique is introduced to analyze the scattered field from an open ended circular cavity (OECC) based on modal Method of Moments. Entire domain cylindrical vector wave functions are employed to express the fields on the cavity aperture and the dyadic Green's functions of the circular cavity is used to formulate the fields inside OECC. At first, scattered field from a perforated OECC in an infinite PEC is calculated by applying the surface equivalence theorem and Galerkin method for solving the resultant integral equation. Then, the scattered field from a hypothetically PEC plate with the size and shape of the circular aperture is added to the previously calculated scattered field to compensate the effect of the infinite PEC assumption. This addition corrects the monostatic RCS results, particularly at close to grazing incident angles.

Monostatic RCS of different size OECCs is calculated and compared with other numerical techniques and measurements. Different sizes are selected in order to demonstrate the capability of the proposed method to evaluate cavities with sizes including resonant size up to several wavelengths. Excellent agreement between the results proves the accuracy of the presented method. Since the method is based on the full wave modal MoM approach, the technique is very efficient for large structures compared to other numerical methods. In addition, further numerical considerations in the formulations have increased the efficiency of the method.

REFERENCES

[1] H. T. Anastassiu, "A review of electromagnetic scattering analysis for inlets, cavities, and open ducts," *IEEE Trans. Antennas Propagat*., vol. 45, no. 6, pp. 27-40, 2003.

[2] J. M. Jin and J. L. Volakis, "A finite element boundary integral formulation for scattering by three dimensional cavity-backed apertures," *IEEE Trans. Antennas Propagat*., vol. 39, no. 1, pp. 97-104, 1991.

[3] J. Liu and J. M. Jin, "A special higher order finite element method for scattering by deep cavities," *IEEE Trans. Antennas Propagat*., vol. 48, no. 5, pp. 694-703, 2000.

[4] W. Rachowicz and A. Zdunek, "An *hp*-adaptive finite element method for scattering problems in electromagnetics," *International Journal of Numerical Methods in Engineering*, vol. 62, no. 9, pp. 1226-1249, 2005.

[5] H. Ling, "RCS of waveguide cavities: A hybrid boundary integral/modal approach," *IEEE Trans. Antennas Propagat*., vol. 38, no. 9, pp. 1413-1420, 1990.

[6] T. T. Chia, R. J. Burkholder, and R. Lee, "The application of FDTD in hybrid methods for cavity scattering analysis," *IEEE Trans. Antennas Propagat*., vol. 43, no. 10, pp. 1082-1090, 1995.

[7] C. A. Chuang and P. H. Pathak, "Ray analysis of modal reflection for three dimensional open-ended

cavities," *IEEE Trans. Antennas Propagat*., vol. 37, pp. 339-346, 1989.

[8] H. S. Ling, W. Lee, and R. C. Chou, "High frequency RCS of open cavities with rectangular and circular cross sections," *IEEE Trans. Antennas Propagat*., vol. 37, no. 5, pp. 648-654, 1989.

[9] A. G. Pino, F. Obelleiro, and J. L. Rodriguez, "Scattering from conducting open cavities by generalized ray expansion (GRE)," *IEEE Trans. Antennas Propagat*., vol. 41, no. 7, pp. 989-992, 1993.

[10] A. Zdunek and W. Rachowicz, "hp-adaptive CEM in practical applications," In Spectral and High Order Methods for Partial Differential Equations, *Springer Berlin Heidelberg*, pp. 339-346, 2011.

[11] A. Zdunek and W. Rachowicz, "Efficient jet-engine inlet radar cross-section prediction using higher-order finite-element method and reduced-order modeling," *Electromagnetics*, vol. 34, pp. 345-362, 2014.

[12] H. R. Witt and E. L. Price, "Scattering from hollow conducting cylinders," *IEE Proceedings*, vol. 115, pp. 94-99, 1968.

[13] H. S. Ling, W. Lee, and R. C. Chou, "High frequency RCS of open cavities with rectangular and circular cross sections," *IEEE Trans. Antennas Propagat*., vol. 37, no. 5, pp. 648-654, 1989.

[14] P. H. Patbak, C. W. Chuang, and M. C. Liang, "Inlet Modeling Studies," Technical Report no. 717674-1, *The Ohio State University Electro Science Laboratory*, Columbus, OH, 1986.

[15] A. Altintas, P. H. Pathak, and M. C. Liang, "A selective modal scheme for the analysis of EM coupling into or radiation from large open-ended waveguides," *IEEE Trans. Antennas Propagat*., vol. 36, pp. 84-96, 1988.

[16] K. K. Chan and F. Tremblay, "Mode matching analysis of metallic blades in a cylinder," *IEEE International Symposium on Antennas and Propagation*, Newport Beach, CA, pp. 38-41, June 18-23, 1995.

[17] A. Zdunek and W. Rachowicz. "Cavity radar cross section prediction," *IEEE Trans. Antennas Propagat*., vol. 56, no. 6, 2008.

[18] C. T. Tai, *Dyadic Green Function in Electro-magnetic Theory*. 2nd edition, New York: IEEE Press, 1994.

[19] L. F. Shampine, "Vectorized adaptive quadrature in MATLAB," *Journal of Computational and Applied Mathematics*, 211, pp. 131-140, 2008.

[20] R. J. Burkholder, P. H. Pathak, and H. T. Chou, "New Ray and Physical Optics Based Methods for Modeling Duct Propagation in the Hybrid Analysis of EM Scattering by Jet Inlets," Technical Report no. 729526–1, *The Ohio State University Electro-Science Laboratory*, Columbus, Ohio, 1995.

[21] C. S. Lee and S. W. Lee, "RCS of a coated circular waveguide terminated by a perfect conductor," *IEEE Trans. Antennas Propagat*., vol. 35, no. 4, pp. 391-398, 1987.

Ali Aghabarati received the B.Sc. degree in Electrical Engineering from Iran University of Science and Technology, Tehran, Iran, in 2008, and the M.Sc. degree in Electrical Engineering from Amirkabir University of Technology, Tehran, Iran, in 2010. He obtained the Ph.D. degree in Computational Electromagnetics from McGill University, Montreal, QC, Canada in 2014. His main research interest is numerical techniques in electro-magnetic computation.

Parisa Dehkhoda was born in Tabriz, Iran, on August 16, 1978. She received the B.S. degree from University of Tehran, Iran, in 2000 and the M.S. and Ph.D. degrees from Amirkabir University of Technology, Tehran, Iran, in 2004 and 2009 respectively, all in Electrical Engineering. She is now an Assistant Professor in Electrical Engineering Department, in Amirkabir University of Technology. Her research interests are EMC, Scattering, and microstrip antennas.

Ahad Tavakoli was born in Tehran, Iran, on March 8, 1959. He received the B.S. and M.S. degrees from the University of Kansas, Lawrence, and the Ph.D. degree from the University of Michigan, Ann Arbor, all in Electrical Engineering, in 1982, 1984, and 1991, respectively.

He is currently a Professor in the Department of Electrical Engineering at Amirkabir University of Technology. His research interests include EMC, scattering of electromagnetic waves and microstrip antennas.